Efficiency of energy transfer, but not external work, is maximized in stunned myocardium

Serge A. I. P. Trines, Cornelis J. Slager, Joost Van der Moer, Pieter D. Verdouw and Rob Krams

Am J Physiol Heart Circ Physiol 279:1264-1273, 2000.

Am J Physiol Heart Circ Physiol
279: H1264–H1273, 2000.

Efficiency of energy transfer, but not external work, is maximized in stunned myocardium

SERGE A. I. P. TRINES, CORNELIS J. SLAGER, JOOST VAN DER MOER, PIETER D. VERDOUW, AND ROB KRAMS
Experimental Cardiology and Hemodynamics Laboratory, Thoraxcenter, Erasmus University Rotterdam, 3000 DR Rotterdam, The Netherlands

Received 17 September 1999; accepted in final form 30 March 2000

Trines, Serge A. I. P., Cornelis J. Slager, Joost van der Moer, Pieter D. Verdouw, and Rob Krams. Efficiency of energy transfer, but not external work, is maximized in stunned myocardium. *Am J Physiol Heart Circ Physiol* 279: H1264–H1273, 2000.—There is no evidence regarding the effect of stunning on maximization of regional myocardial external work (EW) or efficiency of energy transfer (EET) in relation to regional afterload (end-systolic stress, σ_{es}). To that end, we studied these relationships in both the left anterior descending coronary artery (LADCA) and left circumflex coronary artery regions in anesthetized, open-chest pigs before and after LADCA stunning. In normal myocardium, EET vs. σ_{es} was maximal at 75.4 (69.7–81.0)%, whereas EW vs. σ_{es} was submaximal at 12.0 (6.61–17.3) $\times$ 10^2 J/m^3. Increasing σ_{es} increased EW by 18 (10–27)%. Regional myocardial stunning decreased EET (27%) and EW (36%) and caused the myocardium to operate both at maximal EW (EW_{max}) and at maximal EET (EET_{max}). EET and EW became also more sensitive to changes in σ_{es}. In the nonstunned region the situation remained unchanged. Combining the data from before and after stunning, both EW_{max} and EET_{max} displayed a positive relationship with contractility. In conclusion, the normal regional myocardium operated at maximal EET rather than at maximal EW. Therefore, additional EW could be recruited by increasing regional afterload. After myocardial stunning, the myocardium operated at both maximal EW and maximal EET, at the cost of increased afterload sensitivity. Contractility was a major determinant of this shift.

stunning; pig; contractility; regional energy

LEFT VENTRICULAR EXTERNAL WORK (EW) and left ventricular efficiency of energy transfer (EET) have been shown to depend on a complex interplay of afterload, preload, and contractility (20). The individual contribution of these factors to EW and EET may be quantified using the time-varying elastance concept (23). According to this concept, the left ventricular elastance, measured by the instantaneous ratio of pressure over volume (minus the extrapolated volume at zero pressure), changes during a cardiac cycle from a minimal end-diastolic value to a maximal end-systolic value. The latter value (end-systolic elastance, E_{es}) is a measure of contractility (23). The area bounded by the end-diastolic and end-systolic pressure-volume relationships, and the systolic trajectory of the pressure-volume loop is a measure of total left ventricular work, whereas the area within the pressure-volume loop is a measure of left ventricular EW. Left ventricular EET is defined as the ratio of EW over total work.

Several studies have addressed the relationship of power, EW, or EET vs. afterload and have found a maximum in power (20, 25) but not in EET (4). Until now, these relationships have been derived for global heart function, whereas most of the cardiac pathophysiology is associated with regional dysfunction (27). However, to study the energy-afterload relationships during regional dysfunction, it is necessary to apply the physiological concepts on a regional basis. To the best of our knowledge, it is presently unknown whether relationships involving EW, EET, and afterload derived for global hearts are applicable to regional myocardium. Hence, the first aim of the present study was to evaluate in open-chest anesthetized pigs whether maxima in EW and EET, as found in global hearts, are present in regional myocardium in open-chest pigs. As a measure for afterload, we applied regional end-systolic stress (σ_{es}), as arterial properties, e.g., effective arterial elastance, cannot constitute afterload for regional myocardium.

Impairment of global left ventricular function causes the ventricle to deviate from the optimal situation (11, 21). In earlier work, we have shown that, after myocardial stunning, both regional EW and regional EET decreased more than before stunning, when end-systolic pressure was increased (9). In view of the above-mentioned maximum in work, our previous findings may be explained either on the basis of a shift of these maxima to the left or on a change of shape of the EW and EET relationships. Therefore, the second aim of the present study was to evaluate relationships of EW and EET vs. regional afterload before and after producing regional myocardial stunning.

Apart from the question of how regional EW-σ_{es} and EET-σ_{es} relationships are affected by regional stunning, it is presently unknown whether and how stun-

Address for reprint requests and other correspondence: R. Krams, Thoraxcenter, Erasmus Univ. Rotterdam, PO Box 1738, 3000 DR Rotterdam, The Netherlands (E-mail: krams@tch.fgg.eur.nl).

The costs of publication of this article were defrayed in part by the payment of page charges. The article must therefore be hereby marked "*advertisement*" in accordance with 18 U.S.C. Section 1734 solely to indicate this fact.

ning of a region influences the nonstunned region. Hence, we evaluated the relationship of EW-σ_{es} and EET-σ_{es} for the nonstunned region after stunning another region. All of the above-proposed studies were conducted in open-chest pigs with a well-accepted protocol to induce myocardial stunning.

MATERIALS AND METHODS

General. All experiments were performed in accordance with the "Guiding Principles for the Care and Use of Animals" as approved by the Council of the American Physiological Society and under the regulations of the Animal Care Committee of the Erasmus University Rotterdam.

Instrumentation. After an overnight fast, crossbred Yorkshire-Landrace pigs (30–39 kg, $n = 9$) were sedated with 20 mg/kg im ketamine (Apharmo, Arnhem, The Netherlands), anesthetized with 15–20 mg/kg iv pentobarbital sodium (Apharmo), intubated, and connected to a ventilator for intermittent positive-pressure ventilation with a mixture of oxygen and nitrogen (1:2 vol/vol). Arterial oxygen content and blood gases were kept within the normal range [$7.35 < pH < 7.45$; $35 < P_{CO_2}$ (mmHg) < 45; $100 < P_{O_2}$ (mmHg) < 150] by adjusting, when necessary, the respiratory rate and tidal volume. Three 7-French (Fr) fluid-filled catheters were placed in the superior caval veins for the continuous infusion of 10–15 $mg \cdot kg^{-1} \cdot h^{-1}$ pentobarbital sodium, the continuous infusion of saline, the administration of 4 mg of the muscle relaxant pancuronium bromide (Organon Teknika, Boxtel, The Netherlands) prior to thoracotomy, and the administration of the specific negative chronotropic agent zatebradine (1–2 mg/kg, courtesy of Dr. J. W. Dämmgen; Dr. Karl Thomae, Boehringer Ingelheim, Biberach a/d Riss, Germany). Central aortic blood pressure was monitored via an 8-Fr catheter positioned in the thoracic descending aorta, whereas left ventricular pressure and its first derivative were obtained with a 7-Fr micromanometer-tipped catheter (Braun Medical, Uden, The Netherlands), which was inserted via the left carotid artery. A latex balloon made in our laboratory was mounted on a 7-Fr fluid-filled catheter and inserted via the right femoral vein and positioned in the inferior caval vein just above the diaphragm. Inflation of this balloon reduced the preload for the left ventricle. A 7-Fr latex Fogarty catheter (Baxter Healthcare, Irvine, CA) was inserted via the right carotid artery and positioned in the ascending aorta. Inflation of this balloon gradually increased afterload for the left ventricle.

After a midline sternotomy and after ligation of the left mammarian artery and vein, a part of the second left rib was removed, and the heart was suspended in a pericardial cradle. An electromagnetic flow probe (Skalar, Delft, The Netherlands) was placed around the ascending aorta to measure aortic flow. A small segment of the proximal part of the left anterior descending coronary artery (LADCA) was dissected free for placement of an electromagnetic flow probe (Skalar) and an atraumatic clamp to occlude the LADCA. To obtain local coronary venous blood samples, a cannula was inserted into the great cardiac vein, which drains specifically the LADCA perfusion area (2). Pacing leads were attached to the right atrial appendage and connected to a pacing stimulator (model S9; Grass, Quincy, MA). Rectal temperature was monitored throughout the experiment and was maintained between 37°C and 38°C using external heating pads, warming of the saline infusion, and coverage of the animals with blankets.

Two ultrasonic crystals (Triton Technology, San Diego, CA) were positioned in the midmyocardium of both the anterior and posterior left ventricular wall to measure the diameter of the left ventricle. The diameter crystal in the anterior wall was positioned close to the LADCA segment length crystals. The diameter crystal in the posterior wall was positioned such as to optimize signal quality. Two pairs of ultrasonic crystals were implanted in the midmyocardium of the distribution area of the LADCA, each pair 10 mm apart, approximately at one-third of the distance from apex to base. One pair was positioned in the direction of the left ventricular outflow tract (as determined visually), whereas the other pair was placed perpendicular to this direction. The distance of 10 mm and the perpendicularity of the two pairs were assured using a homemade device consisting of two perpendicularly fixed pairs of needles. Similarly, two pairs of crystals were implanted in the midmyocardium of the distribution area of the left circumflex coronary artery (LCXCA), approximately at half the distance from apex to base. One pair was positioned in the direction of the left ventricular outflow tract, and the other pair was placed in the perpendicular direction. The position of the crystals in the midmyocardium was verified at the end of the experiment.

Experimental protocol. After a 30- to 45-min stabilization period, steady-state recordings of hemodynamics and segment lengths in the two myocardial regions were made during 10 respiratory cycles, and global arterial and regional myocardial venous blood samples were collected. After these baseline recordings were made, heart rate was lowered below 70 beats/min by infusion of zatebradine and set at 100 beats/min with the external pacemaker to exclude effects of alterations in heart rate. The baseline measurements were repeated and followed by inflation of the balloon located in the inferior caval vein over a period of 15 s to create a series of 20–25 beats with a gradual reduction of end-systolic left ventricular pressure of ~50–60 mmHg. During the inflation of the balloon, the respirator was switched off. The period of 15 s is sufficiently short to prevent reflex-mediated changes in contractility (1). Moreover, before the heart was paced, systolic, diastolic, and total heart cycle duration did not change in our experiments up to 18 s (for definition of systole and diastole, see below). After hemodynamic variables had resumed preinflation values (differences in mean arterial pressure and in maximum left ventricular pressure rise smaller than 4 mmHg and 100 mmHg/s, respectively), the balloon located in the ascending aorta was then gradually inflated over a period of 10 s to create 10–20 beats with an increase of end-systolic left ventricular pressure of ~30–40 mmHg. The respirator was again switched off during this procedure. The order of inflating the two balloons was randomized for each measurement.

Subsequently, myocardial stunning was produced in the LADCA region by two coronary (LADCA) occlusions of 10 min, separated by 10 min of reperfusion. The last occlusion was followed by 30 min of reperfusion. After this period, the steady-state measurements and the balloon inflations as mentioned above were repeated.

At the end of each experiment, methylene blue was infused into the LADCA, and the myocardium perfused by the LADCA was dissected and weighed. In addition, the myocardium inside the segment crystals in both LADCA and LCXCA regions was also dissected and weighed.

Data acquisition and analysis. Left ventricular pressure, its first derivative, central aortic pressure, aortic flow, coronary blood flow, left ventricular diameter, and the regional segment length signals were digitized (sample rate: 125 Hz) with a 12-bit analog-to-digital converter connected to an AT-based personal computer (AT-CODAS; Keithley Instruments, Gorinchem, The Netherlands) and stored on disk for

offline analysis. Mean arterial pressure, systolic arterial pressure, diastolic arterial pressure, maximum left ventricular pressure rise, left ventricular end-diastolic pressure, cardiac output, stroke volume, and systemic vascular resistance were calculated following standard procedures. Myocardial oxygen consumption of the LADCA perfusion area ($M\dot{V}O_2$, in $J \cdot beat^{-1} \cdot m^{-3}$) was calculated as the product of coronary blood flow and the difference in arterial and coronary venous oxygen content divided by the heart rate and the mass of the LADCA perfusion area. The energy generated by 1 ml of O_2 was set equal to 20 J (22). Left ventricular wall stress (σ, in N/m^2) and strain (ϵ, dimensionless) were calculated offline by applying the formulas described in the APPENDIX. End-systolic stress-strain relationships were determined from the combined pre- and afterload changes by determining left ventricular end-systolic stress-strain points using an iterative fitting algorithm, as described before (26). Briefly, to determine these points, a linear relationship was applied in which elastance was defined as $\sigma/(\epsilon - \epsilon_0)$, where ϵ_0 is the strain at zero wall stress. To initiate the iteration, ϵ_0 was set to zero and elastance was calculated. End-systolic stress-strain points were determined for each heartbeat as the point at which elastance was maximal. Subsequently, a new ϵ_0 value was calculated using a linear least-squares fit through the end-systolic points. The new ϵ_0 value was used to start a new cycle as described above. This procedure was repeated until ϵ_0 did not differ more than 1% from the ϵ_0 determined during the previous cycle. The stress and strain at these points were defined as end-systolic stress (σ_{es}) and end-systolic strain (ϵ_{es}).

As the end-systolic stress-strain relationship was often curvilinear, the end-systolic points were also fitted to the following second-order polynomial regression equation: $\sigma = c_3 \cdot \epsilon^2 + c_2 \cdot \epsilon + c_1$ (14, 26), using the least-squares technique. If the coefficient c_3 was not significantly different from zero ($P \geq 0.05$), the linear equation was selected. If c_3 was negative (concave to the strain axis), the second-order polynomial was selected. If c_3 was positive (convex to the strain-axis) and the fitted curve did not intersect the strain-axis, the data were fitted to the third-order polynomial $\sigma = c_4 \cdot \epsilon^3 + c_3 \cdot \epsilon^2 + c_2 \cdot \epsilon + c_1$. The slope of the end-systolic stress-strain relationship, called the end-systolic elastance (E_{es}, in N/m^2), was used as an index of contractility. As this slope is strain dependent, E_{es} was calculated as the local slope at a stress, corresponding to a left ventricular pressure of 80 mmHg at baseline. This value was identical during the experiment for each pig.

The area enclosed by the left ventricular stress-strain loop during a single heartbeat was calculated as the EW of the myocardial region (in J/m^3), normalized per unit of volume (10, 19, 28). Stress-strain area (SSA, in J/m^3), the regional equivalent of the pressure-volume area (PVA), an index of total ventricular work, was calculated as the area enclosed by the end-systolic and end-diastolic relations and the systolic trajectory of the stress-strain loop (14, 24). Potential energy (PE, in J/m^3) was calculated by subtracting EW from SSA. The regional EET (in %) was calculated as $(EW/SSA) \cdot 100\%$. The situation before pre- and afterload changes was called the working point, and σ_{es}, SSA, EW, PE, and EET at the working point were called $\sigma_{es,wp}$, SSA_{wp}, EW_{wp}, PE_{wp}, and EET_{wp}.

Subsequently, for each animal, EW and EET were plotted versus σ_{es}, and the relationships were normalized such that EW_{wp}, EET_{wp}, and $\sigma_{es,wp}$ were equal to unity before stunning. To account for changes in the coordinates of the working point for σ_{es}, EW, and EET after stunning, the relationships were normalized such that the coordinates of the working point were equal to the ratio of the mean value after stunning and the mean value before stunning. Each relationship was linearly interpolated to obtain a range of equal σ_{es} coordinates for each animal. Maximal EW (EW_{max}), maximal EET (EET_{max}), and their respective σ_{es} values ($\sigma_{es,EWmax}$ and $\sigma_{es,EETmax}$) were determined from the normalized curves. The respective differences between EW_{wp}, EET_{wp}, and $\sigma_{es,wp}$ and EW_{max}, EET_{max}, $\sigma_{es,EWmax}$ and $\sigma_{es,EETmax}$ (ΔEW, ΔEET, $\Delta\sigma_{EW}$, $\Delta\sigma_{EET}$) were determined. Finally, the intervals on the σ_{es} axis (surrounding $\sigma_{es,wp}$), in which EW and EET did not decrease significantly from EW_{wp} and EET_{wp}, were determined using paired *t*-tests. The left and right borders of these intervals are referred to as left and right significance borders. To determine the dependence of EW and EET on σ_{es}, the slopes of the EW-σ_{es} and EET-σ_{es} relationships at these significance borders were calculated. The normalized curves from different animals were averaged at each normalized σ_{es} coordinate showing at least five EW or EET measuring values, and the average curve was filtered applying a moving average filter.

Statistics. For all hemodynamic, contractile, and energetic parameters, the effect of infusion of zatebradine and subsequent pacing at 100 beats/min and of LADCA stunning and, for the contractile and energetic parameters (except $M\dot{V}O_2$), the difference between the LADCA and LCXCA regions was tested by a two-way ANOVA for repeated measurements, followed by Student-Newman-Keuls post hoc tests for multiple comparisons. As $M\dot{V}O_2$ was only measured in the LADCA perfusion area, a one-way ANOVA for repeated measurements was performed. Because we could not describe the EW-σ_{es} and EET-σ_{es} relationships with a regression equation, we could not perform an ANOVA to test for changes in these relationships. To overcome this problem, we applied a three-way ANOVA for repeated measures, using σ_{es}, stunning, and myocardial region as within-subject factors. Because within-subject factors have to be discrete, we divided the range of σ_{es} values in six equal ranges, using the mid-σ_{es} value of each range and the mean of the accompanying EW or EET values. Next, paired *t*-tests were employed for both perfusion areas to test whether ΔEW and ΔEET differed from zero. Paired *t*-tests were also performed to test the influence of LADCA stunning on the parameters of the EW-σ_{es} and EET-σ_{es} relationships.

The influence of E_{es} on the curve parameters EW_{max}, ΔEW, EET_{max}, and ΔEET was tested using linear regression on the pooled data of the LADCA and LCXCA perfusion areas before and after stunning. To validate pooling of the data, the two perfusion areas were encoded using a slope- and an intercept-dummy variable, and significance of these dummies was tested using an *F*-test. For the regressions, one data point with an E_{es} that was 3.7 standard deviations higher than the mean E_{es} was removed. No regression equations are given.

All data have been expressed as means and 95% prediction intervals. $P < 0.05$ was considered significant. Unless stated otherwise, only significant changes are mentioned in the RESULTS.

RESULTS

Systemic hemodynamics. Lowering heart rate by zatebradine from 109 (99–118) beats/min to below 70 beats/min and subsequent pacing to 100 beats/min did not affect any hemodynamic parameter significantly, except for the maximum left ventricular pressure rise, which decreased by 13% (Table 1). Stunning of the LADCA perfusion area decreased diastolic arterial pressure (15%) and the maximum left ventricular pres-

Table 1. *Systemic hemodynamics before and after LADCA stunning*

	Baseline [109 (99–118) beats/min]	Before Stunning (100 beats/min)	After Stunning (100 beats/min)
Mean arterial pressure, mmHg	92(82–102)	89(79–99)	78(67–88)
Systolic arterial pressure, mmHg	108(99–118)	106(96–116)	96(87–105)
Diastolic arterial pressure, mmHg	77(68–85)	74(64–84)	63(53–73)†
Maximum left ventricular pressure rise, mmHg/s	1,730(1,450–2,010)	1,510(1,350–1,660)*	1,240(950–1,530)†
End-diastolic left ventricular pressure, mmHg	9.8(8.2–11.4)	9.0(7.2–10.8)	10.8(8.8–12.8)
Cardiac output, l/min	2.9(2.3–3.5)	2.6(2.3–3.0)	2.0(1.5–2.4)†
Stroke volume, ml	27(22–31)	26(23–30)	20(15–24)†
Systemic arterial resistance, mmHg·min·l^{-1}	34(26–41)	35(28–41)	41(35–48)†

Values are means, with 95% prediction interval in parentheses; $n = 9$ pigs. LADCA, left anterior descending coronary artery. *$P < 0.05$ vs. baseline. †$P < 0.05$ vs. before stunning at heart rate of 100 beats/min.

sure rise (18%). Cardiac output and stroke volume both decreased by 23%, and systemic vascular resistance increased by 17%.

Regional contractile and energetic parameters. At baseline, all contractile and energetic parameters were the same between the LADCA and LCXCA regions, except for SSA_{wp} in the LCXCA region, which was 89% of SSA_{wp} in the LADCA region. Lowering heart rate from 109 to below 70 beats/min and pacing at 100 beats/min had no effect on E_{es}, ϵ_0, $\sigma_{es,wp}$, EW_{wp}, PE_{wp}, and EET_{wp} in both the LADCA and the LCXCA perfusion area, except for SSA_{wp} of the LCXCA perfusion area, which decreased by 15% (Table 2). There was no difference between the LADCA and LCXCA region for any parameter, while $M\dot{V}O_2$ of the LADCA perfusion area was also unaffected. In the LADCA perfusion area, stunning reduced E_{es} by 38%, whereas ϵ_0 increased by 10%. EW_{wp} decreased by 36%, causing a decrease in EET_{wp} of 27%. SSA_{wp} and PE_{wp} remained unchanged, although PE_{wp} tended to increase. Stunning did not affect $M\dot{V}O_2$. Stunning the LADCA perfusion area had no effect on any of the contractile and energetic parameters of the LCXCA perfusion area, except for EW_{wp}, which decreased by 23%. Stunning also induced differences between the LADCA and LCXCA perfusion areas for E_{es}, ϵ_0, PE, and EET.

EW-σ_{es} relationships. Before stunning, the individual EW-σ_{es} relationships displayed a maximum in EW at 14.1 (7.8–20.4) $\times 10^2$ J/m^3 at an σ_{es} of 15.3 (10.1–20.6) $\times 10^3$ N/m^2 (LADCA, before stunning; Fig. 1) and 11.9 (7.9–15.8) $\times 10^2$ J/m^3 at an σ_{es} of 15.9 (12.3–19.5) $\times 10^3$ N/m^2 (LCXCA, before stunning). There was no significant difference between the two curves. The normalized average curves of both the LADCA and LCXCA regions displayed a steep descending relationship during σ_{es} reduction; the slopes of these curves at the left significance border were 3.46 (0.63–6.29) (LADCA) and 2.62 (−0.06–5.30) (LCXCA) (Fig. 2, *A* and *C*). However, they displayed a flat relationship during σ_{es} increments; the slopes of the curves at the right nonsignificant maxima were −0.68 (−1.61–0.26) (LADCA) and −0.83 (−1.84–0.19) (LCXCA). Consequently, a decrease in σ_{es} had a strong influence on EW; only a 2.8% (LADCA) or 1.3% (LCXCA) decrease in σ_{es} from the working point already resulted in a significant decrease in EW. In contrast, an increase in σ_{es} did first result in an increase in EW, but a further increase in σ_{es} did not result in a significant decrease

Table 2. *Regional contractile and energetic parameters before and after LADCA stunning*

		Baseline [109 (99–118) beats/min]	Before Stunning (100 beats/min)	After Stunning (100 beats/min)
E_{es}, $\times 10^4$ N/m^2	LADCA	10.8(7.17–14.4)	11.6(8.84–14.3)	7.21(5.16–9.26)†
	LCXCA	11.9(8.55–15.2)	12.0(8.43–15.5)	12.9(8.12–17.7)‡
ϵ_0	LADCA	0.81(0.78–0.83)	0.81(0.77–0.84)	0.89(0.86–0.92)†
	LCXCA	0.82(0.78–0.85)	0.81(0.77–0.86)	0.83(0.78–0.89)‡
$\sigma_{es,wp}$, $\times 10^3$ N/m^2	LADCA	12.3(7.83–16.8)	11.4(7.45–15.4)	12.8(7.90–17.7)
	LCXCA	11.8(9.10–14.4)	11.0(7.94–14.1)	10.2(7.74–12.6)
SSA_{wp}, $\times 10^2$ J/m^3	LADCA	18.8(10.6–27.0)	16.3(8.70–23.8)	14.1(5.98–22.2)
	LCXCA	16.7(10.8–22.6)‡	14.2(9.15–19.2)*	11.1(6.04–16.1)
EW_{wp}, $\times 10^2$ J/m^3	LADCA	13.7(8.00–19.4)	12.0(6.61–17.3)	7.69(2.86–12.5)†
	LCXCA	11.8(7.35–16.2)	9.75(6.51–13.0)	7.50(4.01–11.0)†
PE_{wp}, $\times 10^2$ J/m^3	LADCA	5.10(2.41–7.78)	4.28(2.00–6.57)	6.38(2.65–10.1)
	LCXCA	4.93(3.05–6.82)	4.43(2.38–6.47)	3.55(1.95–5.16)‡
EET_{wp}, %	LADCA	74.7(69.1–80.4)	75.4(69.7–81.0)	54.7(41.3–68.2)†
	LCXCA	70.8(65.6–75.5)	69.7(65.1–74.2)	67.2(61.4–73.0)‡
$M\dot{V}O_2$, $\times 10^2$ J·beat^{-1}·m^{-3}	LADCA	112(73.9–150)	169(92.8–244)	157(69.9–245)

Values are means, with 95% prediction interval in parentheses; $n = 9$ pigs. E_{es}, end-systolic elastance; ϵ_0, strain at zero stress; subscript "wp" indicates working point; σ_{es}, end systolic stress; SSA, stress-strain area; EW, external work; PE, potential energy; EET, efficiency of energy transfer; $M\dot{V}O_2$, myocardial oxygen consumption; LCXCA, left circumflex coronary artery. *$P < 0.05$ vs. baseline. †$P < 0.05$ vs. before stunning at 100 beats/min. ‡$P < 0.05$ vs. LADCA.

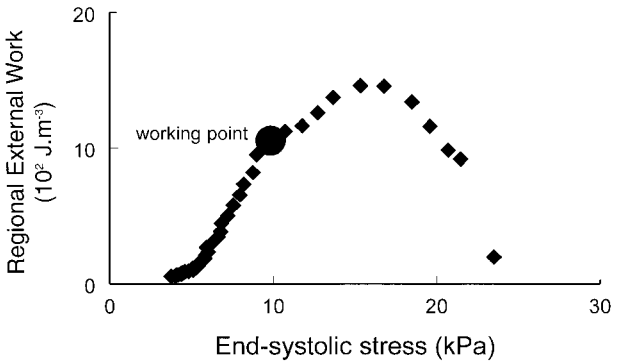

Fig. 1. Example of an EW-σ_{es} relationship of the left anterior descending coronary artery (LADCA) perfusion area before stunning of the LADCA perfusion area. See text for details. EW, external work; σ_{es}, regional end-systolic stress.

in EW. Because of this increase in EW, both $\Delta\sigma_{EW}$ and ΔEW were different from zero; $\Delta\sigma_{EW}$ being 0.35 (0.26–0.45) and 0.39 (0.15–0.64) and ΔEW being 0.18 (0.10–0.27) and 0.21 (0.07–0.34) for the LADCA and LCXCA regions, respectively.

Stunning the LADCA region changed the shape of the EW-σ_{es} curve and shifted it downward (Fig. 2*B*). Therefore, the curves became different between the LADCA and LCXCA regions. Now both a decrease (10%) and an increase (13%) in σ_{es} caused a significant reduction in EW in the LADCA region, whereas in the LCXCA region a 1.1% decrease in σ_{es} still caused a significant decrease in EW and an increase in σ_{es} did not cause a significant decrease in EW. The slopes at the left and right significance border for the LADCA region did not change significantly, however, and remained at 1.86 (1.07–2.65) (*left*) and −1.06 (−2.03 to −0.09) (*right*). Furthermore, $\Delta\sigma_{EW}$ decreased to 0.08 (−0.11–0.27, $P > 0.05$ vs. zero), and ΔEW decreased to 0.07 (0.01–0.13, $P < 0.05$ vs. zero). In addition, the σ_{es} coordinate of the maximum showed a tendency to decrease by 11% [to 13.7 (8.37–19.0) $\times$ 10^3 N/m^2, $P = 0.09$], and the EW coordinate of the maximum of the EW-σ_{es} curve decreased by 39% to 8.65 (3.16–14.1) $\times$ 10^2 J/m^3. For the LCXCA region, the ANOVA showed a significant change in the curve due to LADCA stunning (Fig. 2*D*). However, only EW_{max} decreased by 22% to 9.11 (5.11–13.1) $\times$ 10^2 J/m^3 at an unchanged σ_{es} of 13.1 (11.1–15.1) $\times$ 10^3 N/m^2. The slopes of the curve at the left significance border and the right nonsignificant maximum also remained unchanged at 1.68 (0.27–3.08) and −0.76 (−1.49 to −0.01), respectively.

EET-σ_{es} relationships. The individual EET-σ_{es} relationships displayed a maximum in EET of 78 (74–83)% at an σ_{es} of 10.8 (7.56–14.0) $\times$ 10^3 N/m^2 (LADCA, before stunning, Fig. 3) and at 74 (69–79)% also at an σ_{es} of 10.8 (6.89–14.6) $\times$ 10^3 N/m^2 (LCXCA, before stunning) after changing σ_{es} over a large range of values. There was no significant difference between the two curves. The normalized average curves of both the LADCA and LCXCA regions displayed a flat profile over a relatively large range of σ_{es} values (Fig. 4, *A* and *C*). Outside this region EET decreased more sharply. Therefore, a 25% (LADCA) or 38% (LCXCA) reduction in σ_{es} was necessary to induce a significant decrease in

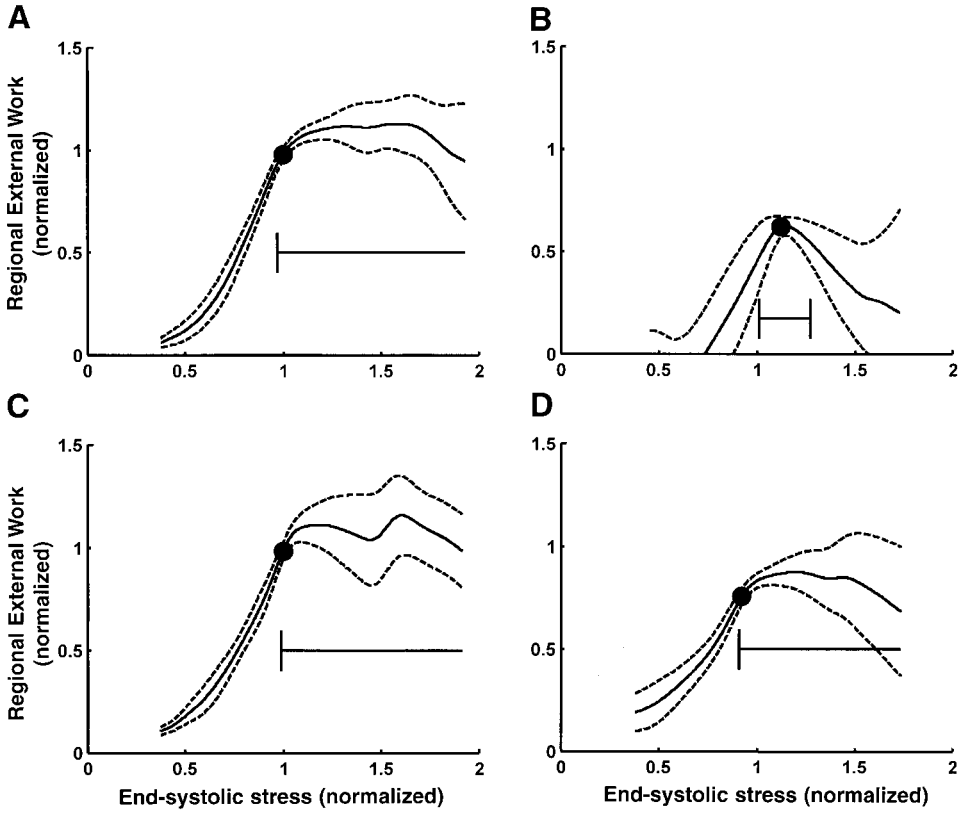

Fig. 2. Averaged curves of normalized EW-σ_{es} relationships. *A*: LADCA before stunning. *B*: LADCA after stunning. *C*: left circumflex coronary artery (LCXCA) before stunning. *D*: LCXCA after stunning. Solid curves are averaged curves; broken lines are 95% prediction intervals. The horizontal line denotes the part of the curve in which EW is not significantly decreased from EW at the working point. If this line extends to the end of the data, no significant decrease in EW was found. See text for details.

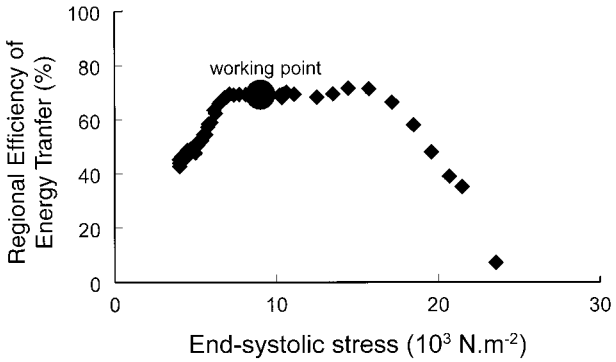

Fig. 3. Example of an EET-σ_{es} relationship of the LADCA perfusion area before stunning of the LADCA perfusion area. See text for details. EET, efficiency of energy transfer.

EET. Also, a 3% (LADCA) or 34% (LCXCA) increase in σ_{es} resulted in a significant decline in EET. The slopes of the curves at the left significance border were 0.54 (0.07–1.02) (LADCA) and 1.01 (−0.15–2.17) (LCXCA). The slopes at the right significance border were −0.10 (−1.09–0.89) and −0.79 (−1.32 to −0.26), respectively. The $\Delta\sigma_{EET}$ was not significantly different from zero, at −0.04 (−0.11–0.04) (LADCA) and −0.04 (−0.17–0.10) (LCXCA). Although the EET coordinates of the working point were different from the maximum ($P < 0.05$), ΔEET was only 0.04 (0.02–0.06) (LADCA) and 0.08 (0.04–0.13) (LCXCA).

Stunning the LADCA region changed the shape of the EET-σ_{es} curve and shifted it downward (Fig. 4*B*). The curve now displayed a maximum at 58.9 (45.7–72.2)% (a decrease of 24%, $P < 0.05$ vs. before stunning), at an σ_{es} of 10.8 (6.46–15.2) × 10^3 N/m^2 ($P > 0.05$ vs. before stunning). Still, a 29% decrease in σ_{es} and a 1% increase in σ_{es} caused EET to decrease significantly. The shape of the EET-σ_{es} curve changed in such a way that EET became more sensitive to both increments and decrements in σ_{es} as the slope of the EET-σ_{es} relationship at the left significance border increased 5-fold to 3.33 (1.33–5.34) and the negative slope at the right significance border increased 19-fold to −1.87 (−3.87–0.12). The $\Delta\sigma_{EET}$ and ΔEET remained unaffected at −0.05 (−0.11–0.01) and 0.07 (0.03–0.12), however. In the LCXCA region, stunning had no significant effect on the EET-σ_{es} curve (Fig. 4*D*). The curve displayed a maximum in EET at 76.6% (66.9–86.4) with an σ_{es} coordinate of 7.86 (5.04–10.7) × 10^3 N/m^2. A decrease in σ_{es} did not cause a significant decrease in EET, but a 0.6% increase in σ_{es} caused a significant decrease in EET. The slope at the left nonsignificant minimum was 1.26 (−3.78–6.30), and the slope at the right significance border was 0.07 (−3.07–3.22).

Relationship with contractility. In the regression between E_{es} and the parameters EW_{max}, EET_{max}, ΔEW, and ΔEET, only EW_{max} and EET_{max} showed a significant positive relationship with E_{es} (Fig. 5). Further analysis revealed that both the relationships between EW_{max} and E_{es} and between EET_{max} and E_{es} were different for the LADCA and LCXCA perfusion areas.

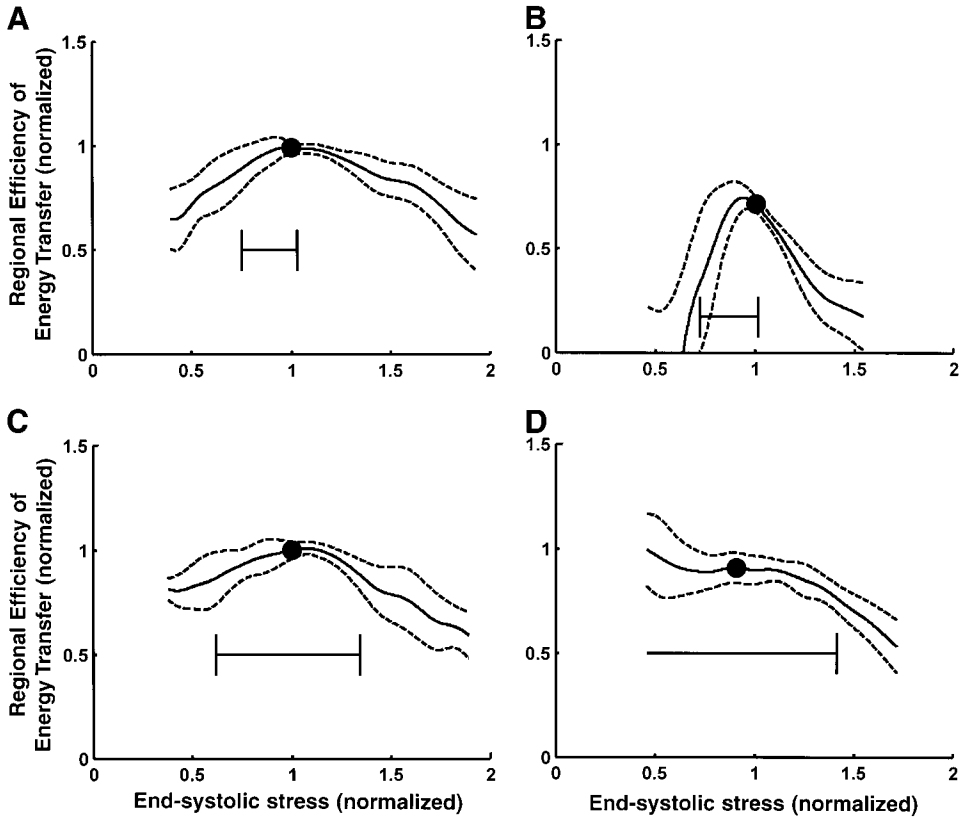

Fig. 4. Averaged curves of normalized EET-σ_{es} relationships. *A*: LADCA before stunning. *B*: LADCA after stunning. *C*: LCXCA before stunning. *D*: LCXCA after stunning. Solid curves are averaged curves; broken lines are 95% prediction intervals. The horizontal line denotes the part of the curve in which EET is not significantly decreased from EET at the working point. If this line extends to the end of the data, no significant decrease in EET was found. See text for details.

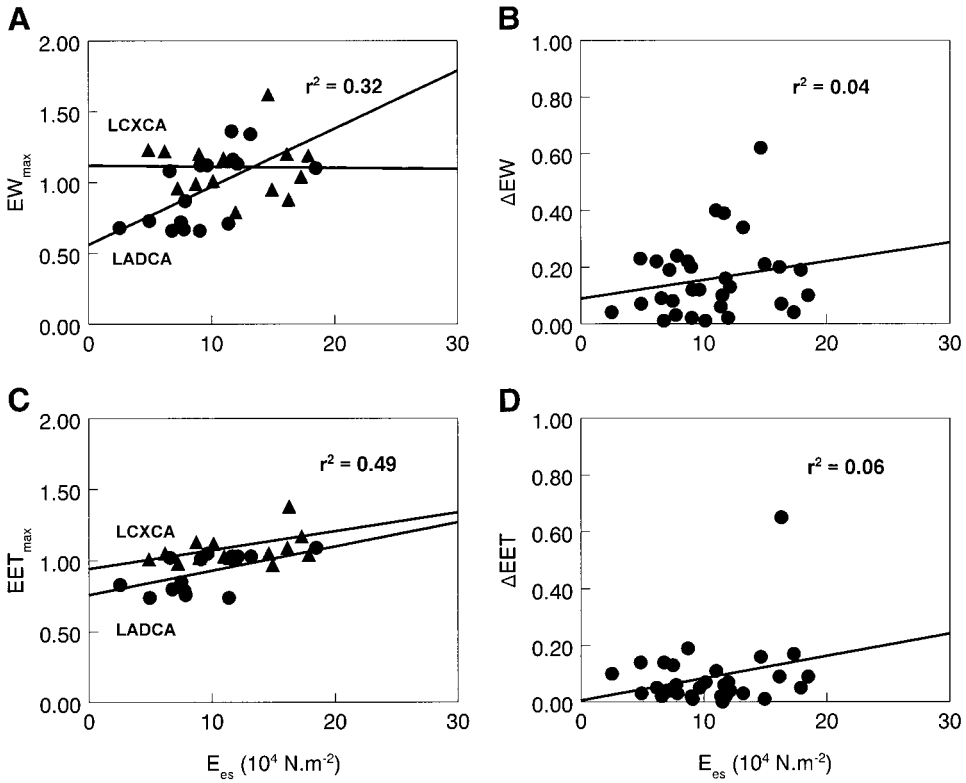

Fig. 5. Relationships between end-systolic elastance (E_{es}) and EW_{max} (*A*), ΔEW (*B*), EET_{max} (*C*), and ΔEET (*D*). Data from before and after stunning and from the LADCA and LCXCA perfusion areas are pooled. For *A* and *C* only, ● = LADCA, ▲ = LCXCA; for *B* and *D*, all data are presented by the same symbol (●). EW_{max}, maximal regional EW; ΔEW, difference between maximal regional EW and regional EW at the working point; EET_{max}, maximal regional efficiency of energy transfer; and ΔEET, difference between maximal regional efficiency of energy transfer and regional efficiency of energy transfer at the working point. See text for details.

DISCUSSION

Normal myocardium. Our first aim was to evaluate whether regional EET and regional EW displayed a maximum in relation to regional afterload, defined as regional σ_{es}. In a strict sense, only EET displayed a maximum in the LADCA and LCXCA perfusion areas, as the relationship between regional EW and afterload showed an increase in EW without a subsequent decrease after increments in afterload. These findings are therefore partly in accordance with earlier studies (5, 7), in which both global EW and EET displayed a maximum and decreased with increasing afterload. A possible explanation for this discrepancy is that in the present in vivo experiments, increments in afterload are accompanied by increments in preload. We investigated the effect of this possible pitfall by dividing EW at the working point and EW at the highest σ_{es} by their respective end-diastolic strains, a measure of regional preload. However, due to the small increments in strain (1.4%), we still could not find a significant decrease in EW at the highest σ_{es}. Therefore, we have to conclude that in the present settings the relationship between EW and afterload increased to a plateau when afterload was increased.

The increase in EW with increasing afterload was 18–20% of the EW at the working point, also when EW was corrected for preload changes. In contrast, maximal EET was only 4–8% different from the EET at the working point, whereas the two σ_{es} values were not different. Therefore, we conclude that in our experiments normal myocardium operated at maximal EET rather than at maximal EW.

There is no consensus on whether global left ventricular power is maximal under physiological conditions. For instance, in a modeling study based on data of intact, conscious dogs, Burkhoff and Sagawa (5) predicted that power is likely to be submaximal. However, if they used data from anesthetized, open-chest dogs, then a maximization of power was predicted. In the present study measurements were performed in anesthetized, open-chest swine, and we therefore expected a maximization of power. However, in anesthetized patients undergoing abdominal surgery, Kadoi et al. (13) found a ventriculo-arterial coupling ratio in agreement with submaximal power. In the same study, patients undergoing coronary artery bypass surgery with a low ejection fraction had a ventriculo-arterial coupling ratio suggesting maximization of power. Consequently, these results indicate that, apart from myocardial dysfunction, species differences may play an important role. To our knowledge, in swine, ventriculo-arterial coupling has only been studied in the normal right ventricle, also suggesting submaximal power (3).

Stunned myocardium. Regional stunning of the LADCA perfusion area decreased contractility in accordance with former studies (14). In addition, end-systolic ϵ_0 increased by 10%. In a former study, we have shown that stunning causes increases in left ventricular volume at zero pressure, independent of inotropic interventions (15). The increase in ϵ_0 may therefore be attributed to a decrease in elastic restoring forces, probably induced by alterations in the extracellular collagen matrix and/or the cytoskeleton.

After stunning the LADCA perfusion area, both EW and EET displayed maxima in relation to σ_{es}. In accordance with decrements in EW and EET at the working point, the maxima in EW and EET were decreased compared with normal myocardium. The maximum of the EW-σ_{es} relationship also tended to shift to the left, but this change was not significant ($P = 0.09$). EW_{max} was now only 7% higher than EW at the working point, and $\sigma_{es,EWmax}$ was no longer different from $\sigma_{es,wp}$ at the working point. As a consequence, the working point was now similar to EW_{max}. To the best of our knowledge, only relative changes in ventriculo-arterial coupling ratio have been reported after regional stunning (30). From these data it cannot be concluded whether power was maximized before or after stunning.

A second effect of stunning was that both EW and EET became more sensitive to increments in afterload. This is in agreement with our former study in which we showed that both EW and EET, deduced from pressure-segment length relationships, decreased more with increasing afterload after myocardial stunning (9). As EET also became more sensitive to decrements in σ_{es}, afterload regulation became more critical in stunned myocardium. Changes in preload did not influence this difference, because preload maximally increased by 4% before stunning and 4.5% after stunning ($P = 0.41$). In the LCXCA perfusion area, however, the relationship between EW at the working point and EW_{max} remained unchanged. So, if we augment global afterload, then EW will increase in the LCXCA perfusion area and decrease in the LADCA perfusion area. Consequently, global afterload will not simultaneously maximize EW in both myocardial regions. Because EET at the working point does not change in relation to EET_{max}, both regions still operate at EET_{max}. However, small changes in afterload will immediately decrease EET in the stunned LADCA perfusion area. From these findings, we conclude that EW and EET are regulated separately in the two myocardial regions, and the LCXCA region does, at least in porcine myocardium, not adapt itself to compensate for the LADCA region.

In accordance with the oxygen consumption paradox of stunned myocardium (8), steady-state myocardial oxygen consumption was unchanged after myocardial stunning. In a former study we showed that two periods of 10 min of ischemia caused ATP, ADP, and total adenine nucleotides to decrease by 34%, 37%, and 33%, respectively, while energy charge [defined as $(ATP + 0.5 \cdot ADP) \cdot (ATP + ADP + AMP)^{-1}$] remained unchanged (17). This suggests an adequate ATP turnover despite a decrease in the concentrations of each high-energy phosphate.

Relationship with contractility. We studied the relationship between E_{es} and EW_{max}, EET_{max}, ΔEW, and ΔEET in the LADCA perfusion area. Although ΔEW was decreased in stunned myocardium, we could not show a positive relationship between ΔEW and E_{es}. A possible explanation might be that the range in ΔEW was too small, because we did find a positive relationship between E_{es} and EW_{max}. This latter result was to be expected, because, apart from ΔEW, EW_{wp} also decreased with myocardial stunning, in accordance with former results (16). In that particular study, we also showed a positive nonlinear relationship between EET_{wp} and E_{es}.

Underlying mechanism. It is well accepted that myocardial stunning is the result of disturbances in excitation-contraction coupling. As a consequence, E_{es} is decreased in stunned myocardium. Because of the positive relationship between E_{es} and EW_{max}, the decrease in E_{es} caused a reduction in EW_{max}. EW_{wp}, however, is not only dependent on contractility but also on the regional afterload, characterized by $\sigma_{es,wp}$. Because regional afterload did not decrease, due to a compensatory increase in systemic vascular resistance (Table 1), EW_{wp} decreased less than EW_{max}, causing the reduction in ΔEW.

Limitations. The present study is based on the time-varying elastance concept, i.e., a single elastance changing over time as a model for the myocardium. Hence, visco-elastic properties, kinetic energy, and the history effect (4, 6, 18) are not accounted for. Although the effect of these properties is considered small under physiological circumstances, their contribution in stunned myocardium is presently unknown. In this respect, the results of this study should be interpreted with caution.

In our in vivo model, we were not able to change preload and afterload independently. Decreasing global left ventricular preload decreases not only regional preload but also regional afterload, because both regional wall thickness and curvature increase. On the other hand, increasing global left ventricular afterload by inflating an intra-aortic balloon decreases cardiac output and therefore increases preload for the next beat. However, changes in preload were small, and correcting for these increments in preload did not change our results significantly.

We used the posterior-anterior diameter to calculate regional stress in both the LADCA and LCXCA perfusion areas, which is not completely correct for the LCXCA perfusion area, especially after stunning. This diameter may increase after stunning, due to stretch of the LADCA perfusion area. Consequently, applying the curvature changes to the LCXCA perfusion area may not be fully correct. However, because σ_{es} was unchanged after myocardial stunning in both perfusion areas and E_{es} did not change in the LCXCA perfusion area, the error introduced was probably negligible.

We assumed that the myocardial volume between the LADCA crystals remained constant before and after induction of stunning. However, Jennings et al. (12) showed that stunning causes about 8% increase in myocardial cell volume due to increased water content. If we assume that in our preparation myocardial volume between the crystals increased by 8% as well, real wall thickness may have increased by 2%. If so, we underestimated stress, E_{es}, and EW before stunning by 2%. However, $\sigma_{es,wp}$ showed a nonsignificant increase due to myocardial stunning, which may be overesti-

mated due to this limitation. Also, the significant decrease in E_{es} and EW due to myocardial stunning may be underestimated. Therefore, this limitation does not seem to affect the reported alterations caused by myocardial stunning.

As we measured regional $M\dot{V}O_2$ by sampling the great cardiac vein, this measurement only reflected tissue $M\dot{V}O_2$ during steady-state conditions, not allowing us to study the relationship between myocardial efficiency ($EW_{wp}/M\dot{V}O_2$) and regional afterload on a beat-to-beat basis. Therefore, it remains unresolved whether in our study the myocardium operated at maximal myocardial efficiency.

This study was performed in pentobarbital-anesthetized swine. Because pentobarbital is known to decrease baseline myocardial contractility and to attenuate cardiovascular reflexes, caution is therefore warranted when the present results are extrapolated to the awake animal.

Conclusions. In this study, regional myocardium before stunning operated at maximal EET rather than at maximal EW, partially in accordance with findings in the global left ventricle. As a consequence, recruitment of EW was possible by increasing regional afterload. After myocardial stunning, the myocardium operated both at maximal EW and at maximal EET. In addition, both EW and EET became more sensitive to afterload. The reduced contractility of stunned myocardium is thought to have an important effect on these relationships.

APPENDIX

To calculate regional stress and regional strain, we used the following approach. We assumed a concentric spherical geometry of both the regional endocardium and epicardium.

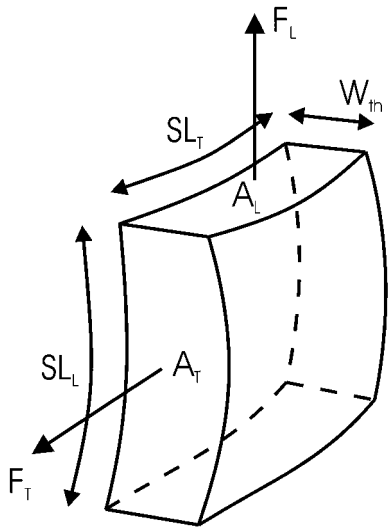

Fig. 6. Schematic representation of the forces working on a block of myocardial tissue. SL_T, transversal segment length; SL_L, longitudinal segment length; W_{th}, wall thickness; A_T, transversal segment area; A_L, longitudinal segment area; F_T, transversal force; and F_L, longitudinal force. For calculations, see APPENDIX.

Wall tension (T) for a sphere, according to Laplace, is

$$T = \frac{P \cdot r}{2} \quad (1)$$

in which P is the cavity pressure and r is the radius of the left ventricle. For a rectangular block of tissue in the ventricular wall between two perpendicularly oriented pairs of crystals, a longitudinal segment length (SL_L, which is in a plane through the long axis of the left ventricle), a transversal segment length (SL_T, perpendicular to SL_L), a force oriented parallel to SL_L (F_L), and a force oriented parallel to SL_T (F_T) are defined (Fig. 6). The equations for the two forces are then

$$F_L = T \cdot SL_T = \frac{P \cdot r \cdot SL_T}{2} \quad (2)$$

and

$$F_T = T \cdot SL_L = \frac{P \cdot r \cdot SL_L}{2} \quad (3)$$

Dividing these forces by the respective areas A_L and A_T delivers the wall stresses in both directions. As the number of fibers producing the forces F_L and F_T being present in the areas A_L or A_T will not change over the cardiac cycle, normalization to fiber stress would not be affected by the changes in the respective areas. We therefore defined a reference state (indicated by the subscript ref) on which all subsequent stress calculations were based. In formula

$$A_{L,ref} = SL_{T,ref} \cdot W_{th,ref} \quad (4)$$

and

$$A_{T,ref} = SL_{L,ref} \cdot W_{th,ref} \quad (5)$$

in which $W_{th,ref}$ is the reference wall thickness. As the volume of the block of tissue (V_{ref}) remains constant during the cardiac cycle, $W_{th,ref}$ can also be written as

$$W_{th,ref} = \frac{V_{ref}}{SL_{T,ref} \cdot SL_{L,ref}} \quad (6)$$

Dividing *Eq. 2* by *Eq. 4*, and *Eq. 3* by *Eq. 5*, and combining with *Eq. 6* gives us

$$\sigma_L = \frac{P \cdot r \cdot SL_T \cdot SL_{L,ref}}{2 \cdot V_{ref}} \quad (7)$$

and

$$\sigma_T = \frac{P \cdot r \cdot SL_L \cdot SL_{T,ref}}{2 \cdot V_{ref}} \quad (8)$$

in which σ_L and σ_T are the longitudinal and transversal wall stress, respectively. Mean average wall stress was defined as the geometric mean (29) according to

$$\sigma_{mean} = \sqrt{\sigma_L \cdot \sigma_T} = \frac{P \cdot r}{2 \cdot V_{ref}} \cdot \sqrt{SL_{L,ref} \cdot SL_{T,ref}} \cdot \sqrt{SL_T \cdot SL_L} \quad (9)$$

Similarly, mean regional strain (ϵ) was derived from the geometric mean according to

$$\varepsilon = \frac{\sqrt{SL_T \cdot SL_L}}{\sqrt{SL_{T,ref} \cdot SL_{L,ref}}} \quad (10)$$

The technical assistance of Jan R. van Meegen and Rob H. van Bremen is gratefully acknowledged.

REFERENCES

1. **Aversano T, Maughan WL, Hunter WC, Kass D, and Becker LC.** End-systolic measures of regional ventricular performance. *Circulation* 73: 938–950, 1986.
2. **Bier J, Sharaf B, and Gewirtz H.** Origin of anterior interventricular vein blood in domestic swine. *Am J Physiol Heart Circ Physiol* 260: H1732–H1736, 1991.
3. **Bolliger C, Fourie P, and Coetzee A.** The effect of prostaglandin E_1 on acute pulmonary artery hypertension during oleic acid-induced respiratory dysfunction. *Chest* 99: 1501–1506, 1991.
4. **Burkhoff D, De Tombe PP, and Hunter WC.** Impact of ejection on magnitude and time course of ventricular pressure-generating capacity. *Am J Physiol Heart Circ Physiol* 265: H899–H909, 1993.
5. **Burkhoff D and Sagawa K.** Ventricular efficiency predicted by an analytical model. *Am J Physiol Regulatory Integrative Comp Physiol* 250: R1021–R1027, 1986.
6. **Crozatier B.** Stretch-induced modifications of myocardial performance: from ventricular function to cellular and molecular mechanisms. *Cardiovasc Res* 32: 25–37, 1996.
7. **De Tombe PP, Jones S, Burkhoff D, Hunter WC, and Kass DA.** Ventricular stroke work and efficiency both remain nearly optimal despite altered vascular loading. *Am J Physiol Heart Circ Physiol* 264: H1817–H1824, 1993.
8. **Dean EN, Shlafer M, and Nicklas JM.** The oxygen consumption paradox of "stunned myocardium" in dogs. *Basic Res Cardiol* 85: 120–131, 1990.
9. **Fan D, Soei LK, Sassen LM, Krams R, and Verdouw PD.** Mechanical efficiency of stunned myocardium is modulated by increased afterload dependency. *Cardiovasc Res* 29: 428–437, 1995.
10. **Goto Y, Suga H, Yamada O, Igarashi Y, Saito M, and Hiramori K.** Left ventricular regional work from wall tension-area loop in canine heart. *Am J Physiol Heart Circ Physiol* 250: H151–H158, 1986.
11. **Ishihara H, Yokota M, Sobue T, and Saito H.** Relation between ventriculoarterial coupling and myocardial energetics in patients with idiopathic dilated cardiomyopathy. *J Am Coll Cardiol* 23: 406–416, 1994.
12. **Jennings RB, Schaper J, Hill ML, Steenbergen C Jr, and Reimer KA.** Effect of reperfusion late in the phase of reversible ischemic injury. Changes in cell volume, electrolytes, metabolites, and ultrastructure. *Circ Res* 56: 262–278, 1985.
13. **Kadoi Y, Kawahara H, and Fujita N.** The end-systolic pressure-volume relationship and ventriculoarterial coupling in patients undergoing coronary artery bypass graft surgery. *Acta Anaesthesiol Scand* 42: 369–375, 1998.
14. **Krams R, Duncker DJ, McFalls EO, Hogendoorn A, and Verdouw PD.** Dobutamine restores the reduced efficiency of energy transfer from total mechanical work to external mechanical work in stunned porcine myocardium. *Cardiovasc Res* 27: 740–747, 1993.
15. **Krams R, Janssen M, Van der Lee C, Van Meegen J, De Jong JW, Slager CJ, and Verdouw PD.** Loss of elastic recoil in postischemic myocardium induces rightward shift of the systolic pressure-volume relationship. *Am J Physiol Heart Circ Physiol* 267: H1557–H1564, 1994.
16. **Krams R, Soei LK, McFalls EO, Winkler Prins EA, Sassen LM, and Verdouw PD.** End-systolic pressure length relations of stunned right and left ventricles after inotropic stimulation. *Am J Physiol Heart Circ Physiol* 265: H2099–H2109, 1993.
17. **Lamers JM, Duncker DJ, Bezstarosti K, McFalls EO, Sassen LM, and Verdouw PD.** Increased activity of the sarcoplasmic reticular calcium pump in porcine stunned myocardium. *Cardiovasc Res* 27: 520–524, 1993.
18. **Milnor WR.** Ventricular work. In: *Hemodynamics* (2nd ed.). Baltimore, MD: Williams and Wilkins, 1989, p. 282–290.
19. **Morris, J Jr, Pellom GL, Murphy CE, Salter DR, Goldstein JP, and Wechsler AS.** Quantification of the contractile response to injury: assessment of the work-length relationship in the intact heart. *Circulation* 76: 717–727, 1987.
20. **Myhre ES, Johansen A, Bjornstad J, and Piene H.** The effect of contractility and preload on matching between the canine left ventricle and afterload. *Circulation* 73: 161–171, 1986.
21. **Nichols WW and Pepine CJ.** Ventricular/vascular interaction in health and heart failure. *Compr Ther* 18: 12–19, 1992.
22. **Sagawa K, Maughan L, Suga H, and Sunagawa K.** Energetics of the heart. In: *Cardiac Contraction and the Pressure-Volume Relationship*. New York: Oxford University Press, 1988, p. 171–231.
23. **Sagawa K, Maughan L, Suga H, and Sunagawa K.** Experimental search for time-varying elastance concept. In: *Cardiac Contraction and the Pressure-Volume Relationship*. New York: Oxford University Press, 1988, p. 55–69.
24. **Suga H, Hisano R, Hirata S, Hayashi T, Yamada O, and Ninomiya I.** Heart rate-independent energetics and systolic pressure-volume area in dog heart. *Am J Physiol Heart Circ Physiol* 244: H206–H214, 1983.
25. **Toorop GP, Van den Horn GJ, Elzinga G, and Westerhof N.** Matching between feline left ventricle and arterial load: optimal external power or efficiency. *Am J Physiol Heart Circ Physiol* 254: H279–H285, 1988.
26. **van der Velde ET, Burkhoff D, Steendijk P, Karsdon J, Sagawa K, and Baan J.** Nonlinearity and load sensitivity of end-systolic pressure-volume relation of canine left ventricle in vivo. *Circulation* 83: 315–327, 1991.
27. **Verdouw PD, van den Doel MA, de Zeeuw S, and Duncker DJ.** Animal models in the study of myocardial ischaemia and ischaemic syndromes. *Cardiovasc Res* 39: 121–135, 1998.
28. **Vinten-Johansen J, Gayheart PA, Johnston WE, Julian JS, and Cordell AR.** Regional function, blood flow, and oxygen utilization relations in repetitively occluded-reperfused canine myocardium. *Am J Physiol Heart Circ Physiol* 261: H538–H547, 1991.
29. **Weast RC, Astle MJ, and Beyer WH.** *CRC Handbook of Chemistry and Physics* (66th ed.). Boca Raton, LA: CRC, 1985, p. F-83.
30. **Yokoyama Y, Novitzky D, Deal MT, and Snow TR.** Facilitated recovery of cardiac performance by triiodothyronine following a transient ischemic insult. *Cardiology* 81: 34–45, 1992.